Conformational Analysis of Glutathione in Aqueous Solution with Molecular Dynamics

Outi Lampela,‡ André H. Juffer,‡ and Arvi Rauk*,†

Department of Chemistry, The University of Calgary, Calgary, Alberta, Canada T2N 1N4 and Biocenter and Department of Biochemistry, University of Oulu, P.O. Box 3000, FIN-90014 University of Oulu, Finland

Received: April 30, 2003

Molecular dynamics simulations over 20 ns with the Gromacs all-atom force field, coupled with cluster analyses of the trajectories, have been applied to the sixteen charge states of glutathione (GSH) in order to examine the distribution conformations in aqueous solution as a function of pH. The simulations show that GSH is very flexible and does not adopt a strongly preferred conformation at any pH. Comparison with limited conformational data deduced from NMR analyses shows little agreement. Contrary to the NMR results which found essentially equal populations of the three rotameric forms, the simulations reveal lower populations for gauche rotameric forms of the Cys and Glu side chains. In most species, the lowest populations were found for the sterically hindered gauche−gauche orientation about the $C_\alpha-C_\beta$ bond in both residues, except when electrostatic attraction between oppositely charged ends, unshielded by intervening water, was found to dominate. In the majority of the enzyme-bound GSH structures extracted from the Brookhaven Protein Data Bank, the bound GSH has a conformation that is either the same or similar to that free in solution. In some cases, as in the case of solid-state GSH and the oxidized form, GSSG, crystal packing and intermolecular H-bonding interactions force the GSH skeleton into a conformation that is not seen in solution. The distribution of the separation of the Cys S atom from the Glu $^{\alpha}C-H$ bond was monitored over the course of the 20 ns simulations to deduce conditions under which H atom transfer may occur from the Glu $^{\alpha}C-H$ bond to a thiyl radical of the Cys moiety of GSH, as has been observed experimentally.

Introduction

Glutathione (γ-glutamylcysteinylglycine, GSH, is a ubiquitous tripeptide which plays a number of vital roles in cell metabolism,

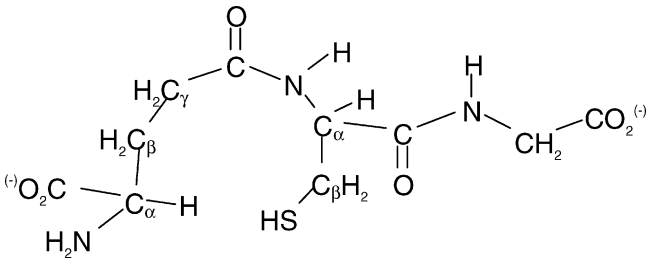

including repair of oxidative damage in erythrocytes and elsewhere.[1] It is the reduced cofactor of glutathione peroxidase, which, like catalase, removes H_2O_2. The oxidized form, glutathione disulfide (GSSG), is reduced to GSH by the action of glutathione reductase and NADPH. GSH is a free radical scavenger in the central nervous system and has been suggested to function as a redox modulator of ionotropic receptor activity, and possibly as a neurotransmitter.[2] Decreased GSH levels have been associated with increased oxidative stress in various neurological disorders including Lou Gehrig's disease (ALS), Parkinson's disease, and Alzheimer's disease.[2]

A continued interest in our research is in the properties of thiyl radicals and the possibility that such radicals may propagate damage to the $^{\alpha}C$-site of peptides and proteins by H atom abstraction.[3,4] Such transfer of damage has been shown experimentally in the case of glutathione, in which the thiyl radical can abstract the H atom from the $^{\alpha}C$-site of the glutamyl residue.[5−7] We have investigated this process computationally.[8] In that case, ab initio methods were employed and an examination was made of the effects of aqueous solution on the energetics of the H atom transfer pathways using continuum models. It was not possible to include explicit effects of solvation by ab initio methods, due to the large size of GSH itself. Nor is it possible by these methods to obtain a satisfactory description of the solution conformational space of any of the charged species, or to examine the balance between the different charge states as a function of pH. We here adopt empirical molecular modeling methods to investigate these aspects of the solution structure of GSH.

The structure of GSH has been determined by single-crystal X-ray analysis in isolation[9,10] and bound to a variety of proteins.[11,12] NMR techniques have been applied to determine the structure of free GSH in aqueous solution as a function of pH,[13,14] and also as bound to several proteins.[15,16] In addition, a number of conformations of the singly charged form in the gas phase have been determined by semiempirical (PSILO) calculations.[17] The structures and relative energies of three neutral forms of GSH in the gas phase and in solution (modeled by continuum methods) have been reported at the ab initio B3LYP/6-31G(d) level of theory.[8]

Due to the presence of the two carboxylic acid groups, the thiol group, and the amino group, sixteen different charged species with net charges ranging from +1 to −3 are available to GSH. The charged states are labeled **1**−**16** in Figure 1 and are accompanied by a string of four symbols, +, −, or 0, in parentheses, which identify the net charge (from left to right) of the terminal amino group, the glutamyl carboxylate group,

* Corresponding author.
† University of Calgary.
‡ University of Oulu.

10.1021/jp030556j CCC: $25.00
Published on Web 10/07/2003

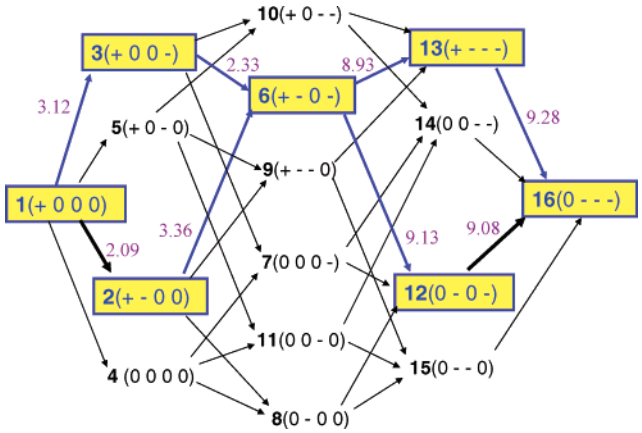

Figure 1. Definition of the charged states of GSH: (q1 q2 q3 q4) designates net charge at the glutamyl N, glutamyl carboxyl, cysteinyl sulfur, and glycyl carboxyl groups, respectively. Arrows indicate single deprotonation steps. Values on the arrows are micro-pK_a values (ref 13).

the thiol group of the cysteine residue, and the terminal glycyl carboxylate group. Thus **6**(+ − 0 −) is the species that is zwitterionic at the glutamyl residue, has the cysteine moiety in the neutral thiol (S−H) form, and in which the glycyl carboxylic acid has been deprotonated. The net charge of **6** (+ − 0 −) is −1. The sixteen species are connected by single proton gain or loss as seen in Figure 1. NMR studies of the aqueous solution of GSH have been used to identify the seven highlighted species in Figure 1 and partially assign the micro-pK_a values of the COOH, NH_3^+, and SH groups.[13,18] The fractional populations of the species highlighted in Figure 1 as a function of pH were also determined.[13]

Partial conformational analyses of GSH were conducted by NMR spectroscopy at various acidity values.[14,18] The predominant conclusion from the NMR studies is that all species interconvert rapidly among a wide variety of conformations, but that motion of the glutamyl backbone was restricted by interaction of its α-amino and α-carboxy groups with the γ-Glu-Cys peptide carbonyl and N−H, respectively. Populations of several rotameric forms were deduced from spin−spin coupling analysis.[14,18] These are discussed below in connection with the results of our simulations.

Each of the species **1**−**16** shown in Figure 1 may exist in numerous conformations. The conformational space of a particular species in aqueous solution may be determined by molecular dynamics (MD) simulations. From the results of the simulations, one may derive the relative free energies of the different conformers of a given species. The relative solution free energies of *different* species cannot be determined in such a straightforward manner because information about the strengths of individual bonds is lacking from the empirical force field. The determination of relative solution free energies, and hence pK_a values, is beyond the scope of the present work.

We have adopted the Gromacs all-hydrogen force field for the MD simulations. The Gromacs all-hydrogen force field is a successor to the Gromos/87 force field, which has been applied to many simulations of biomolecules. These include both large[19−24] and small peptides[25−29] in the gaseous phase,[26,29] in water solutions,[22−25,27,28,] in membranes,[20,21] and in interactions with enzymes.[30,31] Comparisons with NMR data have been previously reported at least by van der Spoel in studies of Gly-X-Gly peptides,[25] and by Smith et al. on aspects of hen lysozyme structure.[19]

Computational Details

Molecular dynamics simulations of the 16 different charge states of GSH were carried out with Gromacs3.05[32] suite of programs using the Gromacs all hydrogen force field. In the deprotonated cysteine residue, a charge of −1 was placed on the sulfur atom. The initial conformation was taken from a previous 1 ns simulation of one of the GSH charge states.[33] All of the protonation states were created from the initial conformation using Gromacs programs. Each of the conformations was placed into a cubic box and solvated by approximately 400 SPC water molecules.[34] Counterions (Na^+ or Cl^-) were added to the box if the total charge of the peptide was nonzero to satisfy the electroneutrality condition. All of the conformations were energy minimized using a steepest descent method, and a short position-restraining simulation was carried out restraining the peptide in order to relieve close contacts before the actual simulation.

For each of the 16 GSH charged species, one or more 20 ns simulations were performed with a time step of 2 fs. Weak coupling to a temperature (300 K) and pressure (1 bar) bath was employed.[35] For long-range electrostatics, the particle mesh Ewald (PME) summation[36] was applied with grid spacing of 0.12 nm and fourth-order interpolation. For van der Waals interactions, a 0.9 nm cutoff was used. The LINCS[37] and SETTLE[38] algorithms were employed to satisfy the bond constraints of the peptide and water molecules, respectively. The center of mass motion was removed at every step, and the neighbor list was updated on every tenth step. The atom coordinates were recorded into a trajectory file every 1 ps. The conformations of each charge state, and their relative populations, were extracted from the resulting 16 trajectories.

Identification of Conformations and Determination of their Relative Free Energies. The conformations were extracted from the trajectories by the "clustering method".[39] The root-mean-square deviations (RMSD) of peptide heavy atom coordinates of each frame were calculated against those from every tenth frame, implying a time difference between analyzed frames of 10 ps, in order to identify configurations (atom coordinates in the frame) that are structurally similar. The RMSD = 0.075 nm criterion was deemed sufficient to distinguish between adjacent torsional conformers. The peptide configuration that had the most configurations inside a 0.075 nm RMSD criterion was taken to be the center of the first "cluster". All the configurations closer than the criterion were taken into that cluster. The procedure was repeated for the remaining configurations until all the configurations were clustered (assigned to one conformation or another). Each cluster identifies a separate conformation.

The free-energy of each conformation, **b**, relative to the first (most abundant) conformation, **a**, is calculated according to the respective fractional populations, p_a and p_b:

$$\Delta G_b = -k_B T \ln(p_b/p_a) \qquad (1)$$

where k_B is the Boltzmann constant, T is the temperature, and the fractional population, p_a, of a conformation, **a**, is the number of configurations assigned to that conformation by the clustering method, divided by the total number of configurations (typically about 2000).

Results and Discussion

For each of the charged species (Figure 1), a 20 ns molecular dynamics simulation was carried out. In the case of **1**(+ 0 0 0) and **6**(+ − 0 −), the simulations were rerun from different starting points. Similar results were obtained, indicating that

TABLE 1: Fractional Populations of the Ten Most Stable Conformations of Each Charge State of GSH

species		charge	mole fraction of conformers										$\Delta G_{300}^{\circ a}$ kJ/mol
		q	**a**[b]	**b**	**c**	**d**	**e**	**f**	**g**	**h**	**i**	**j**	
1	(+ 0 0 0)	+1	0.10	0.07	0.07	0.07	0.03	0.03	0.03	0.03	0.03	0.03	3.0
2	(+ − 0 0)	0	0.10	0.06	0.06	0.06	0.05	0.05	0.03	0.03	0.03	0.02	4.0
3	(+ 0 0 −)	0	0.13	0.09	0.06	0.06	0.05	0.05	0.03	0.03	0.02	0.02	4.7
4	(0 0 0 0)	0	0.05	0.05	0.04	0.04	0.04	0.04	0.03	0.03	0.02	0.02	2.3
5	(+ 0 − 0)	0	0.16	0.14	0.09	0.05	0.05	0.04	0.04	0.03	0.03	0.03	4.2
6	(+ − 0 −)	−1	0.12	0.11	0.08	0.07	0.03	0.03	0.03	0.03	0.02	0.02	4.5
7	(0 0 0 −)	−1	0.13	0.05	0.04	0.04	0.04	0.03	0.03	0.02	0.02	0.02	4.7
8	(0 − 0 0)	−1	0.06	0.06	0.05	0.05	0.05	0.03	0.03	0.02	0.02	0.02	2.7
9	(+ − − 0)	−1	0.20	0.14	0.06	0.05	0.05	0.04	0.03	0.03	0.03	0.03	4.7
10	(+ 0 − −)	−1	0.38	0.13	0.11	0.07	0.04	0.03	0.02	0.02	0.02	0.02	7.3
11	(0 0 − 0)	−1	0.17	0.15	0.13	0.12	0.11	0.04	0.03	0.02	0.02	0.02	5.3
12	(0 − 0 −)	−2	0.07	0.05	0.04	0.04	0.03	0.03	0.03	0.03	0.03	0.02	3.1
13	(+ − − −)	−2	0.25	0.12	0.08	0.04	0.03	0.03	0.03	0.03	0.02	0.02	6.3
14	(0 0 − −)	−2	0.26	0.13	0.10	0.06	0.05	0.03	0.03	0.02	0.02	0.02	6.4
15	(0 − − 0)	−2	0.24	0.12	0.07	0.04	0.04	0.02	0.02	0.02	0.02	0.02	6.2
16	(0 − − −)	−3	0.07	0.06	0.05	0.04	0.04	0.04	0.03	0.03	0.03	0.02	3.1

[a] Free energy difference between conformer **j** and conformer **a**. [b] See Table 2 and Figure 2 for definition of conformer **a**.

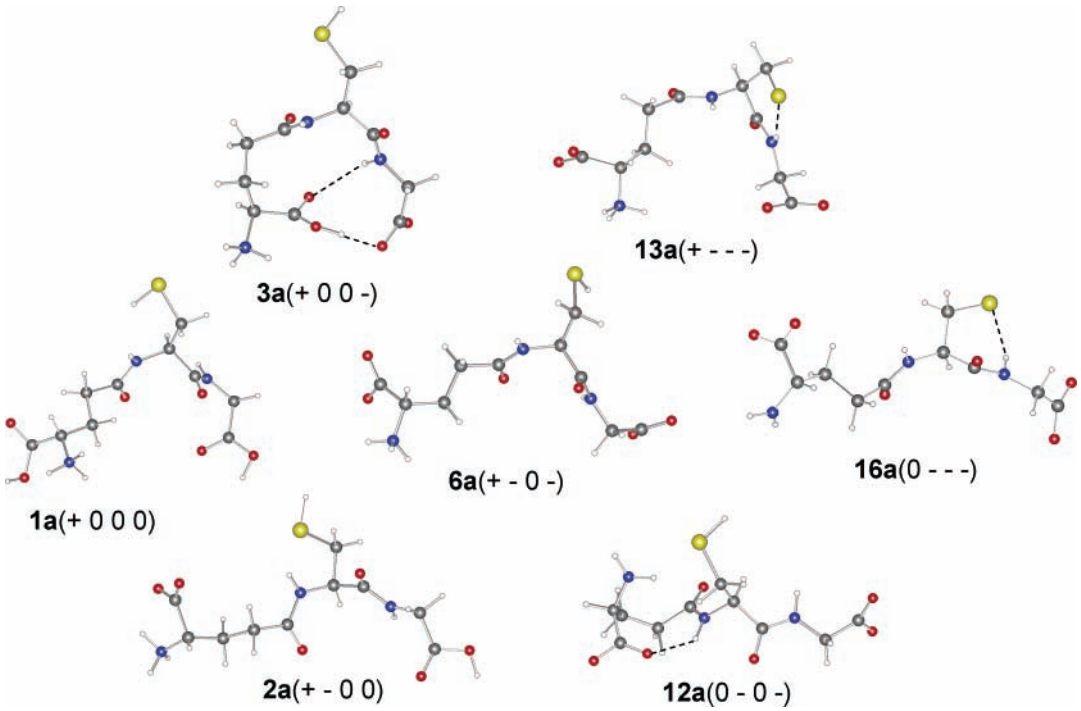

Figure 2. Structures of the most abundant conformations of the species highlighted in Figure 1.

these species were well equilibrated in the 20 ns span of the simulation. Cluster analysis revealed that most visited more than a hundred conformations during the course of the simulation. The fractional populations of the 10 most abundant conformers of each of the 16 charged states of GSH (Figure 1) are given in Table 1. For convenience, the free energy difference calculated by eq 1 between the first and tenth conformer is listed in the last column. It is immediately evident from inspection of the data of Table 1 that, in the majority of cases, there is little preference for any single conformer. Thus, any macroscopic measurement such as NMR of an aqueous solution must necessarily pertain to an average over many conformers. This consideration will be evident in the discussion below of literature deductions of conformational distributions based on NMR measurements. The narrow range of relative solution free energies of 1−2 k_BT (last column of Table 1) also means that almost any shape may be adopted with little penalty. The relevance of this consideration will be apparent in the discussion below of the comparison between the solid-state structures of free and protein-bound GSH and the situation in solution.

The structures of the most stable conformations of the seven species of GSH highlighted in Figure 1 are shown in Figure 2. An example of the immediate hydration environment is shown in Figure 3 in the case of **6**(+ − 0 −). The fifteen closest water molecules are all within 3 Å of one of the charged groups or a polar bond of one of the two amide groups. The sulfhydryl group (−SH) behaves as a hydrophobic group and is not immediately solvated. The ammonium group has a single water molecule with its dipole pointed to the end of each of the N−H bonds, as expected for a normal H-bond. Such a structure is also seen in the case of the N−H bond of an amide group and the OH of a protonated carboxylate, if present. It must be remembered that in most molecular mechanics force fields, an H-bond is described purely as an electrostatic attraction, with no charge transfer component. In the case of polar or charged oxygen atoms of GSH, the water molecules tend to orient with one OH

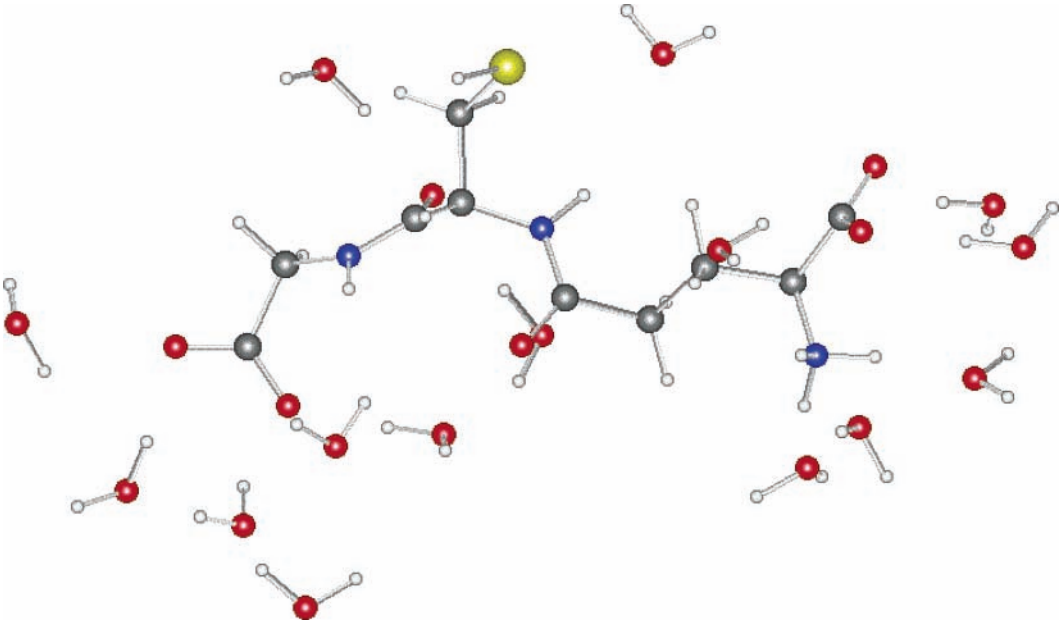

Figure 3. Structure of **6b**(+ − 0 −) showing the nearest solvation shell (water within 3 Å of the closest non-H atom)

bond directed toward the oxygen, but because of the purely electrostatic nature, there is no directional preference for the "H-bond" relative to the electron-pair donor except that imposed by the rest of the charge distribution.

Conformational Analysis. Conformational flexibility will in part be determined by the distribution of charged and polar groups in the molecule. In the gas phase, the number of available conformers is severely curtailed by intramolecular Coulombic repulsion or attraction and the possibility or lack thereof, of intramolecular H-bond formation. This situation may be radically different in a polar solvent such as water. A simple measure of the conformational flexibility of GSH is a monitoring of some internal separation, for example, the end-to-end distance, as a function of the simulation time. For three species, **1**(+ 0 0 0), **3**(+ 0 0 −), and **6**(+ − 0 −), the most stable conformations are shown in Figure 4a. The minimum separation of the terminal amino and carboxy groups of each species is displayed over the course of 20 ns simulations in Figure 4b. In all three species the amino group is protonated placing a positive charge at one end. For **1**(+ 0 0 0), the distance-time correlation plot (Figure 4b) shows a random distribution weighted near 1 nm (10 Å), with no obvious preference for a "folded" conformation, which would bring the oppositely charged groups into closer proximity. The histogram in Figure 4c shows the fraction of total time spent at different distance intervals. The distribution for **1**(+ 0 0 0), shows that it exists about 25% of its time with the separation of the end groups in the interval 9−10 Å. In **3**(+ 0 0 −), the glycyl carboxy group is also ionized, placing a negative charge at the other end. Comparison of the plots in Figs 4b and 4c for **1**(+ 0 0 0) and **3**(+ 0 0 −) provides insight to the extent to which the Coulombic attraction of the two ends is felt in the presence of discrete water molecules. The distance−time correlation plot (Figure 4b) shows that structures in which the end-to end distance is between 0.4 and 0.6 nm (4 Å − 6 Å) persist for long intervals of time. This is dramatically evident in the histogram plot for **3**(+ 0 0 −) which has two peaks in structures in the interval, 4−6 Å, corresponding to about 30% of the simulation time. Structure **6**(+ − 0 −) is zwitterionic at the glutamyl moiety. The distance−time correlation (Figure 4b) and histogram (Figure 4c) plots are very similar to those of **1**(+ 0 0 0), an indication that the intervening water molecules can shield the weaker charge−dipole interaction between the charged carboxylate group and the neutral but zwitterionic opposite end.

Conformational Analysis in Terms of Dihedral Angle Distributions. For three GSH torsional angles, NMR spin−spin coupling analyses have been applied to provide information about the populations of different conformers. These are the side chain angle, $NC_\alpha C_\beta S$, of Cys, and two backbone angles, $NC_\alpha C_\beta C_\gamma$ and $C_\alpha C_\beta C_\gamma C$, of the Glu moiety. These torsion angles are defined in Figure 5, as are the Ramachandran angles of the cysteine moiety (ϕ(Cys) and ψ(Cys)) and the glycine moiety (ϕ(Gly)).

According to Rabenstein,[13] the seven GSH structures (charge species) that are highlighted in Figure 1 dominate at different values of pH. These are **1**(+ 0 0 0), **2**(+ − 0 0), **3**(+ 0 0 −), **6**(+ − 0 −), **12**(0 − 0 −), **13**(+ − − −), and **16**(0 − − −). Structural data in the form of the internal dihedral angles (Figure 5) are given in Table 2 for the most stable conformation of each (see also Figure 2). The corresponding rotamer distributions were derived from the simulations for each of these seven species and are shown in Figures 6−12, respectively.From the Newman projection of the $NC_\alpha C_\beta S$ angle of the cysteinyl moiety (Figure 5), it is evident that +60° corresponds to the sterically most crowded gauche−gauche conformer, while at 180° and −60°, the backbone amide N or C, respectively, are in the less crowded position anti to the S atom. Perusal of the distribution function for this angle in Figures 6−12, reveals that the −60° rotamer is favored in species **1**(+ 0 0 0), **2**(+ − 0 0), **3**(+ 0 0 −), and **6**(+ − 0 −), and that the +60° rotamer is the least populated. This situation is dramatically reversed in the case of **13**(+ − − −) where the population of the +60° rotamer is 76%. In this conformation, the negatively charged S atom forms an H-bond with the N−H bond of the cysteinyl moiety.

Similar considerations apply to the $NC_\alpha C_\beta C_\gamma$ dihedral angle of the glutamyl moiety. The most hindered rotamer, +60°, with all gauche interactions of the large groups, has virtually no population in six of the seven species considered, the exception being **12**(0 − 0 −) (Figure 10). In the case of **12**(0 − 0 −), steric hindrance of this rotamer is compensated by the formation of an intramolecular H-bond between the negatively charged

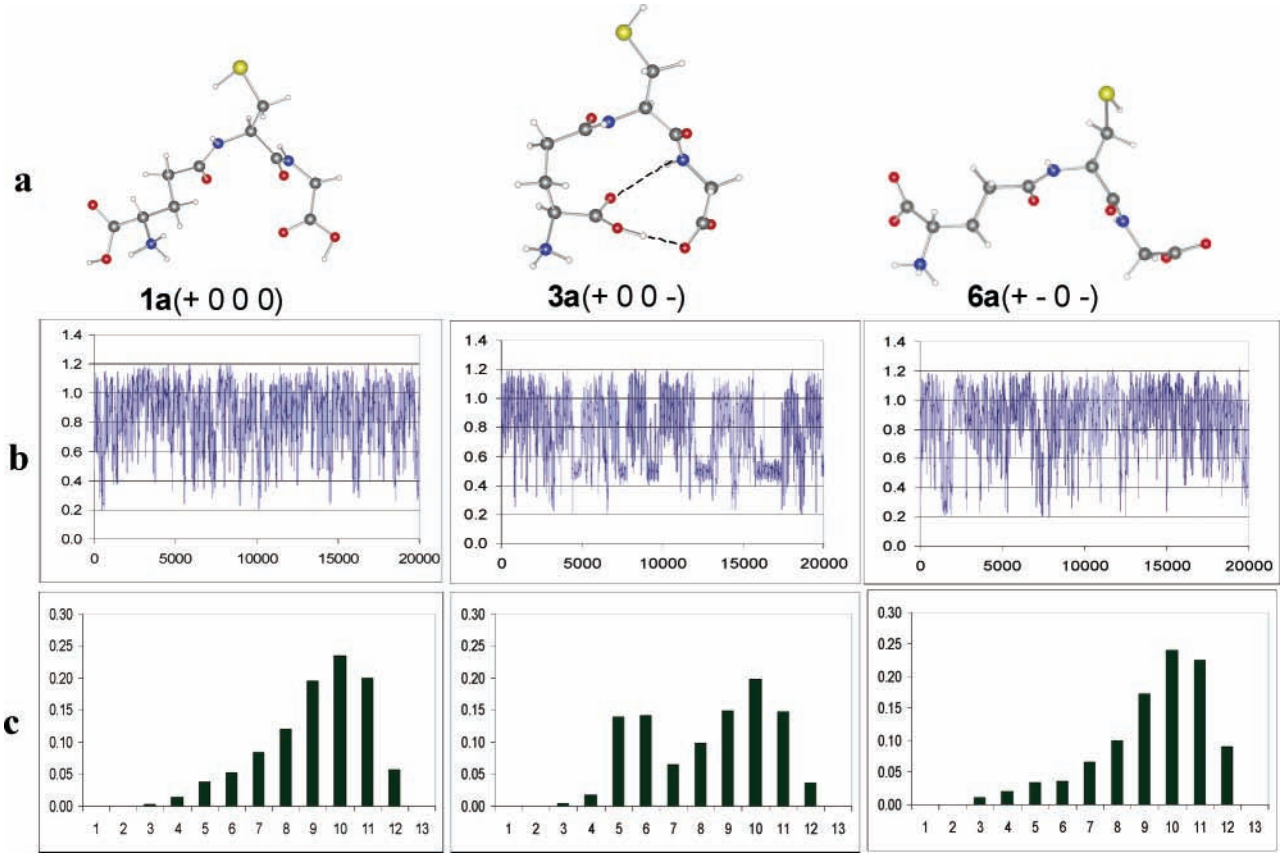

Figure 4. (**a**) Structures with different charged end groups; (**b**) Minimum distance of the terminal $NH_3^{(+)}$ and $CO_2^{(-)}$ groups during the course of the simulation; vertical axis = distance in nm, length of horizontal axis = 20 ns; (**c**) Histograms of the minimum distance of the terminal $NH_3^{(+)}$ and $CO_2^{(-)}$ groups: vertical axis = fraction of total simulation time; bins correspond to 1 Å intervals.

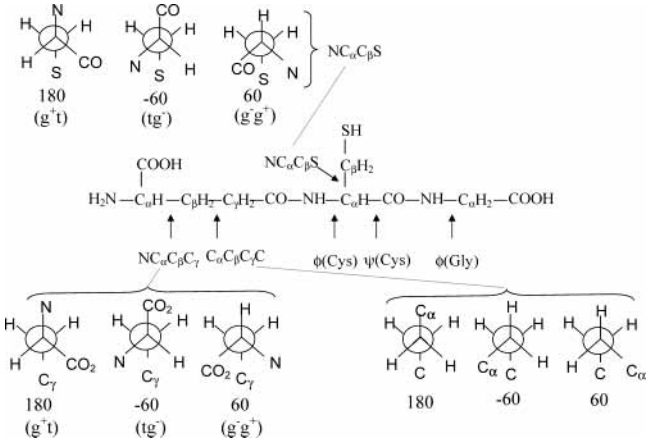

Figure 5. Definition of dihedral angles discussed in the text and in Figures 6−12.

glutamyl carboxylate group and the N−H bond of the proximal amide group (see **12a**(0 − 0 −) in Figure 2).

The $C_\alpha C_\beta C_\gamma C$ dihedral angle of the glutamyl moiety (Figure 5) is not as hindered. The most stable form should be 180°, in which the distal C atoms are anti to one another. Indeed, this rotamer is dominant in all of the species (Figures 6−12) except **12**(0 − 0 −). The gauche forms (−60° and/or +60°) have appreciable populations due to intramolecular H-bond formation in species **3**(+ 0 0 −), **12**(0 − 0 −), **13**(+ − − −), and **16**(0 − − −). Examples are shown in Figure 2.

Comparison to NMR Data. Glutathione in solution is a mixture of different protonation states at all but very low and very high pH where only the totally protonated or totally unprotonated forms of glutathione, i.e., **1**(+ 0 0 0) and **16**(0 − − −), respectively, exist. We discuss first the structures at low and high pH, and then at physiological pH in terms of their relationship to NMR data from the investigations of Fujiwara et al.,[18] and York et al.[14]

Low pH: **1**(+ 0 0 0). At pH = 0, the only structure with appreciable abundance is **1**(+ 0 0 0), but at pH = 1, species **2**(+ − 0 0) comprises about 10% of the mixture.[13] Fujiwara et al. concluded that the three cysteinyl conformers were equally populated at low pH (and all pH < 8). This was later revised by York et al. who concluded that at pH = 1.2, the cysteinyl side chain rotation adopts *two* dominant conformations, 42% of $NC_\alpha C_\beta S$ = +60°, and 44% of either 180° or −60°. The present analysis suggests that the 180° conformer should be dominant (50%) and that only 10% of the mixture at pH = 1.2 should have $NC_\alpha C_\beta S$ = +60°.

York et al. found approximately equal populations of the three rotamers about the $NC_\alpha C_\beta C_\gamma$ dihedral angle of the glutamyl moiety. Fujiwara deduced a slight excess of the 180° and −60° forms and less of the gauche−gauche +60° form. Both results are in stark contrast with the present work, which finds 60%−70% population of 180°, no significant population for +60°, even after the simulation was restarted from a +60° form.

Fujiwara, et al. also found approximately equal populations of rotamers about the $C_\beta C_\gamma$ bond ($C_\alpha C_\beta C_\gamma C$ angle) of the glutamyl moiety. By contrast, the present work finds that approximately 70% of the mixture consists of the 180° conformer.

High pH: **16**(0 − − −). At pH = 11−14, the only structure with appreciable abundance is **16**(0 − − −).[13] Fujiwara et al. found 29% of the $NC_\alpha C_\beta S$ = +60° cysteine rotamer and unequal populations, 48% and 23%, of the other two conformers, 180° or −60°, which could not be distinguished. This pattern

TABLE 2: Dihedral Angles of the More Stable Solution Conformers of GSH and of Experimental Solid State and Enzyme-Bound Structures

species		charge	dihedral angle (deg)[a]					
		q	$NC_\alpha C_\beta S$	$NC_\alpha C_\beta C_\gamma$	$C_\alpha C_\beta C_\gamma C$	ϕ(Cys)	ψ(Cys)	ϕ(Gly)
1a	(+ 0 0 0)	+1	−76.4	−168.5	−176.4	−53.0	117.8	55.0
2a	(+ − 0 0)	0	−53.6	−170.4	−170.1	−97.8	127.7	150.4
3a	(+ 0 0 −)	0	−67.1	−169.5	−69.0	−114.0	84.7	152.2
6a	(+ − 0 −)	−1	−96.1	−165.8	−175.7	−87.9	106.0	−132.8
6b	(+ − 0 −)	−1	−60.8	−73.5	−179.1	−96.1	128.4	140.6
6c	(+ − 0 −)	−1	179.8	−153.8	166.3	−109.0	157.2	102.8
6d	(+ − 0 −)	−1	168.2	−172.6	176.8	−111.2	112.2	160.0
6e	(+ − 0 −)	−1	172.7	−71.0	174.4	−109.4	116.4	−179.2
6f	(+ − 0 −)	−1	−57.4	−162.6	−179.1	−96.1	128.4	−140.6
6 g	(+ − 0 −)	−1	−74.3	−175.9	178.0	−94.5	94.2	112.7
6h	(+ − 0 −)	−1	−58.2	−149.1	169.6	−73.3	109.3	112.0
6i	(+ − 0 −)	−1	−73.9	−144.6	70.0	−99.0	119.3	178.8
6j	(+ − 0 −)	−1	−62.9	170.8	164.4	−90.5	−49.0	−140.8
12a	(0 − 0 −)	−2	−79.5	77.9	−56.6	−125.4	137.3	178.6
13a	(+ − − −)	−2	56.6	−179.0	167.5	−91.1	−70.4	−169.8
16a	(0 − − −)	−3	−173.1	−76.1	−172.0	−112.6	153.7	159.3
			Crystal Structures					
GSH (GLUTAS02)[b]		0	69.9	−70.8	−68.8	−86.9	−3.0	−87.8
GSSG (BERLOZ)[c]		0	−46.6	−73.9	−177.9	−125.6	14.0	−85.2
			Enzyme−bound Structures[d]					
1f2e[e]	−1	−63.2	−174.7	179.0	−132.4	127.6	−128.7	= **6f**(+ − 0 −)
1gsy[e]	−1	−59.7	163.7	177.1	−151.5	155.4	113.4	≈ **6d**(+ − 0 −)
1ljr[e]	−1	−87.3	−179.8	−179.3	−85.7	136.1	92.4	= **6h**(+ − 0 −)
1pmt[e]	−1	−58.4	174.3	174.3	−113.3	120.2	−135.4	= **6f**(+ − 0 −)
2pmt[e]	−1	−60.2	176.5	178.0	−114.4	117.9	−135.8	= **6f**(+ − 0 −)
6gss[e]	−1	−51.5	−175.7	−174.0	−141.2	142.5	111.0	≈ **6c**(+ − 0 −)
7gss[e]	−1	−55.2	−158.5	172.5	−132.9	142.7	117.7	≈ **6c**(+ − 0 −)
19gs[e]	−1	−40.4	−168.2	177.3	−131.8	151.6	101.3	≈ **6c**(+ − 0 −)
1fhe[e]	−1	−106.9	150.8	−77.5	−148.3	69.4	157.1	
6gsy[e]	−1	−32.2	−154.8	173.3	−123.1	6.4	−100.0	
1hnl[f]	−1	−77.9	47.8	148.3	−87.8	159.8	148.7	
1jzr[g]	−1	−74.7	−153.2	179.2	−87.2	148.3	124.8	= **6h**(+ − 0 −)
1*k*0n[g]	−1	28.5	−161.9	170.0	−112.8	174.2	163.7	≈ **6c**(+ − 0 −)
1flj[h]	−1	−76.3	64.9	−173.5	−111.4	−170.2	−108.6	
1gsa[i]	−1	−42.4	−72.3	−172.5	−86.7	104.9	−178.2	≈ **6e**(+ − 0 −)
1pd2[j]	−1	−65.5	−169.7	−175.3	−107.8	167.9	95.2	≈ **6c**(+ − 0 −)
1b4q[k]	−1	−23.6	−51.6	−124.0	62.2	−153.8	141.0	
3grx[l]	−1	−37.5	−76.7	167.8	−83.6	129.6	−171.1	= **6e**(+ − 0 −)

[a] See Figure 5 for definitions of dihedral angles. [b] CSD entry, ref 10. [c] CSD entry, ref 40. [d] PDB entry ID − crystal structures, except 1b4g and 3grx which are NMR structures: = positive assignment to a solution cluster; ≈ based on backbone atoms (excluding $NC_\alpha C_\beta S$). [e] Glutathione S-transferase. [f] Lysozyme (E. C. 3.2.1.17) C77A mutant. [g] URE2 protein. [h] Carbonic anhydrase III. [i] Glutathione synthase. [j] Hematopoietic prostaglandin D synthase. [k] Human thiol transferase (NMR structure, model 4). [l] Glutaredoxin 3 (NMR structure, model 1).

was found to persist at all pH > 8.8. The present data for **16**(0 − − −) (Figure 12) are in qualitative agreement with the higher pH regime in that the populations of the +60° and 180° forms are found to dominate, although less (7%) is found of the −60° form.

However, the agreement fails at lower pH. At pH = 9, the mixture consists of about equal parts of **6**(+ − 0 −), **12**(0 − 0 −), and **16**(0 − − −), with about 35% of **13**(+ − − −). Because each of these species has a unique distribution of rotamers, a pH dependence of rotamer populations is predicted. The appropriately weighted average of these four species from the present simulation suggests that the +60° form of the cysteine side chain rises to 43%, the 180° form falls to 28%, and the −60° form rises to 27% as the pH falls from 14 to 9. Spin−spin coupling analysis did not detect a change in populations about $NC_\alpha C_\beta S$ in this pH range.[18]

In the analysis of Fujiwara, et al., the population distribution about the $NC_\alpha C_\beta C_\gamma$ angle of the glutamyl moiety was difficult to determine but the data were interpreted as indicating substantial, if not equal, populations of each of the three rotameric forms at high pH. In fact, we find the +60° form to be virtually unpopulated in the case of **16**(0 − − −) (Figure 12), i.e., at pH = 14, and at pH = 9, the weighted average of the +60° form only rises to 9%. A significant shift occurs between the 180° and −60° forms, from 18% and 81%, respectively, at pH = 14, to 50% and 40%, respectively, at pH = 9.

In the case of the $C_\alpha C_\beta C_\gamma C$ torsion angle of the glutamyl fragment, Fujiwara et al. were able to monitor the anti (180°) form as a function of pH but could not distinguish the two gauche forms. They found 60% of the 180° form at their highest pH (2 M NaOH), with the population falling monotonically to 34% at the lowest pH (6 M HCl). At pH 9, it was 42%. The present simulation finds the opposite behavior, the population of the 180° form being 50% at pH = 14, rising to 58% at pH = 9, and continuing to rise to 77% at pH = 7 where **6**(+ − 0 −) (Figure 9) is expected to be the dominant form of GSH.[13]

Physiological pH: **6**(+ − 0 −). In the pH range 5−7, a solution of GSH consists almost entirely of **6**(+ − 0 −). Thus, the properties of **6**(+ − 0 −) are expected to be of the greatest importance under physiological conditions. Both Fujiwara et al.[18] and York et al.[14] examined GSH by NMR at pH near 7. We discuss here primarily the work of York and co-workers,

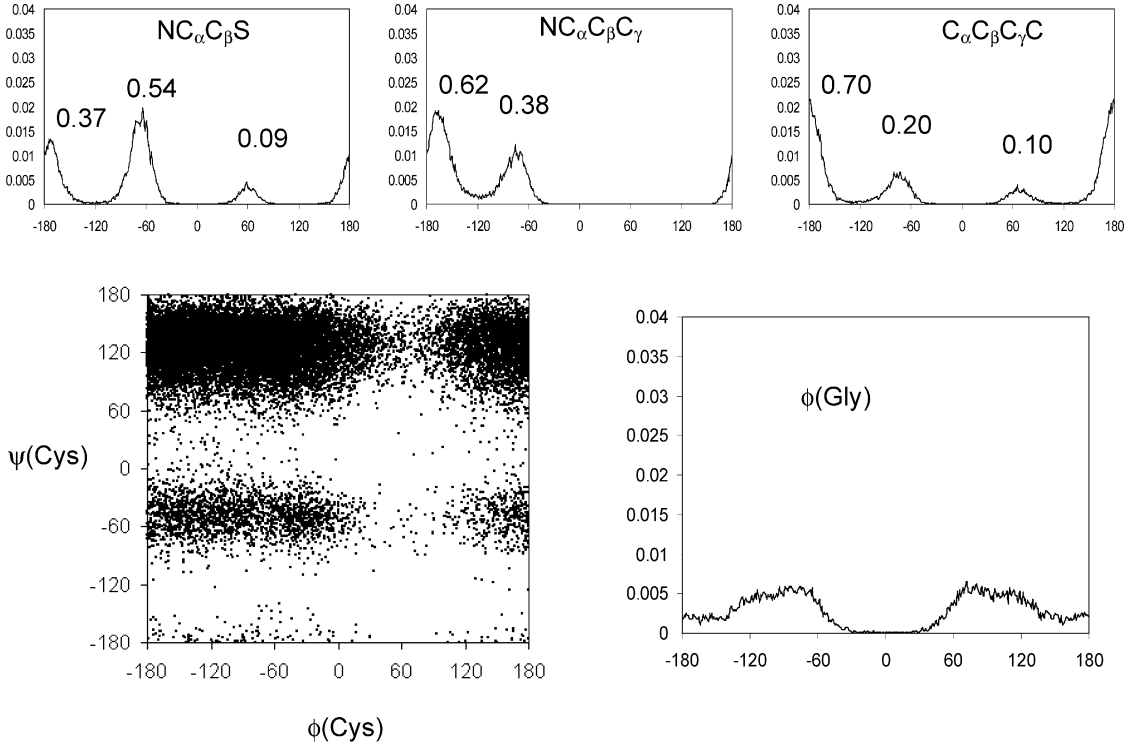

Figure 6. Structure **1**(+ 0 0 0): distribution by dihedral angles (See Figure 5 for definitions).

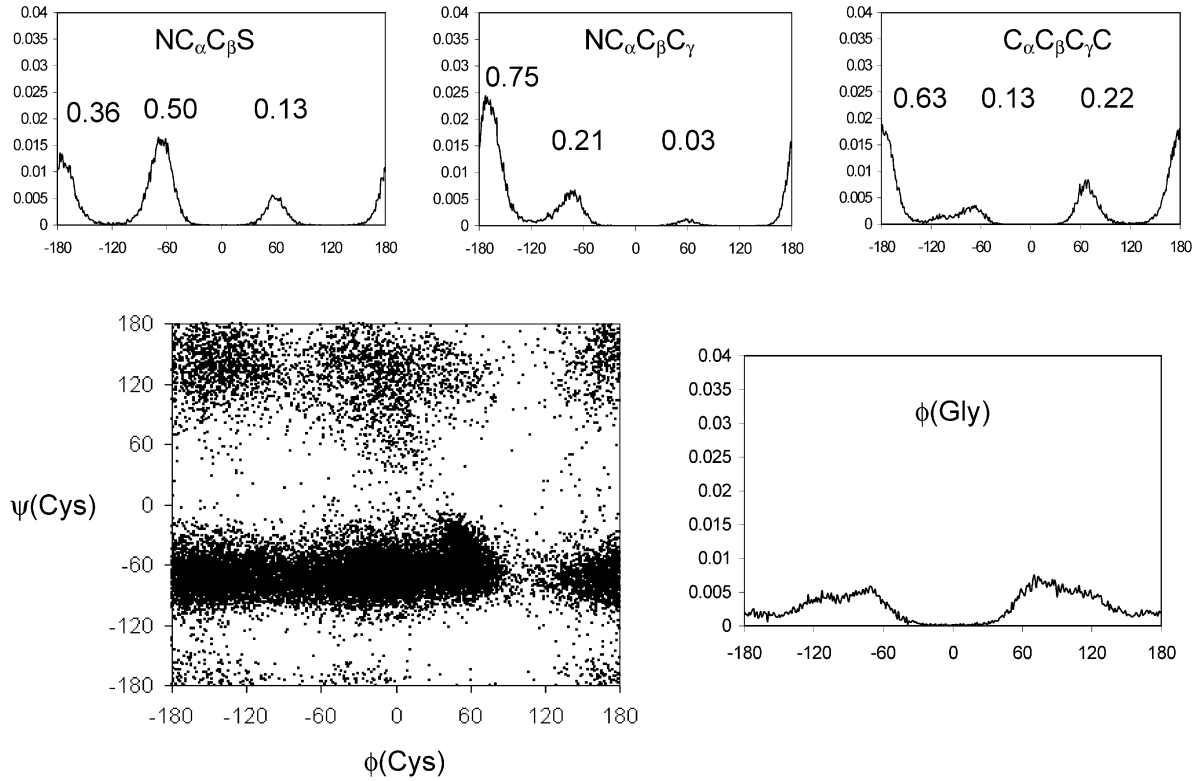

Figure 7. Structure **2**(+ − 0 0): distribution by dihedral angles (See Figure 5 for definitions).

as theirs is the later work and was based on spectral simulations rather than *J* coupling analysis.

For the cysteinyl moiety, York, et al., found 34% population of the $NC_\alpha C_\beta S = +60°$ rotamer, and 44% and 22% populations of the other two forms, although it was not possible to say which was which. The present analysis of **6**(+ − 0 −) finds only 12% (Figure 9) of the +60° rotamer, but finds unequal populations, 53% and 33%, of the 180° and −60° forms, respectively.

York and co-workers only analyzed the population distribution about the $NC_\alpha C_\beta C_\gamma$ angle of the glutamyl residue, finding populations, 30%, 35%, and 35%, respectively, for the +60°, 180°, and −60° forms (although they could not distinguish the latter two). As already mentioned above, the finding of a significant population of the most sterically hindered +60° rotamer is at odds with the present results, namely <1%. The other two forms are also unequally populated, 77% and 22%,

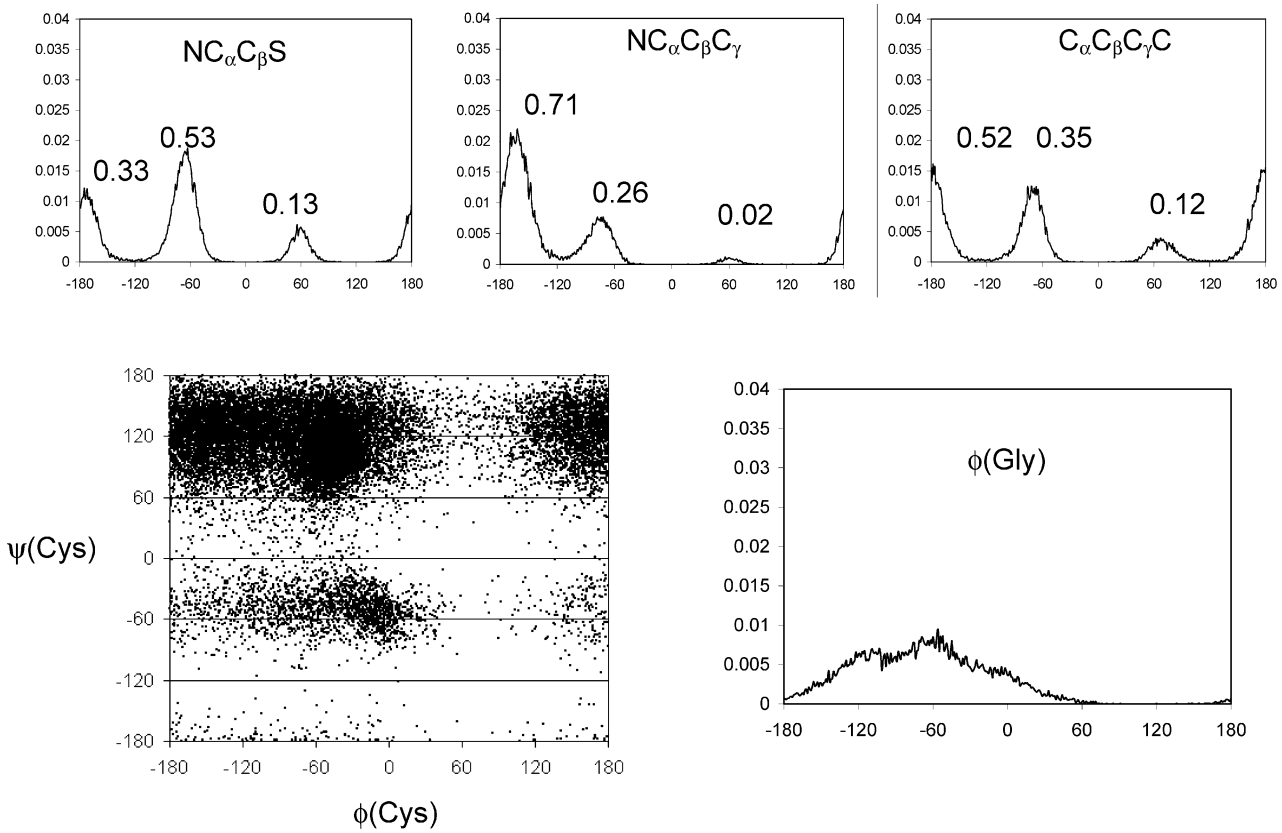

Figure 8. Structure **3**(+ 0 0 −): distribution by dihedral angles (See Figure 5 for definitions).

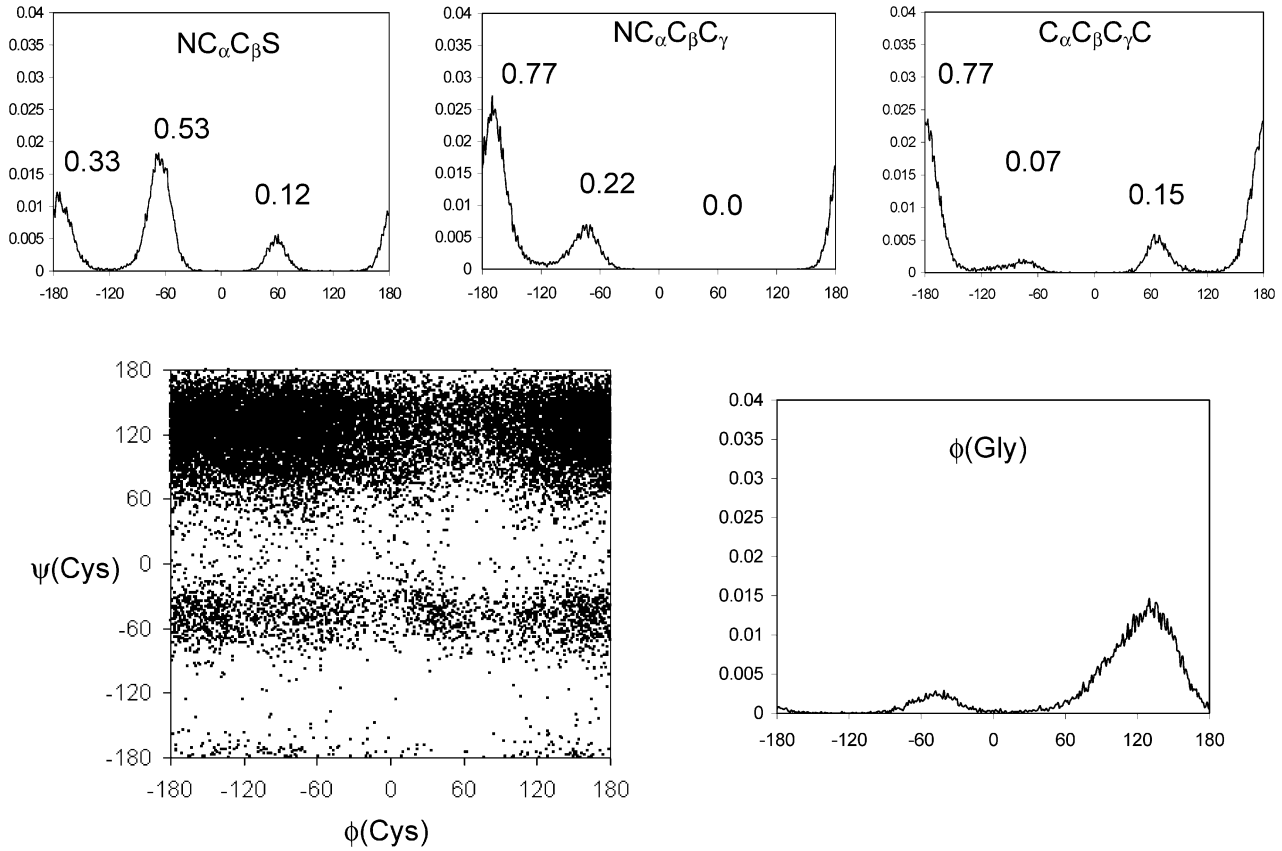

Figure 9. Structure **6**(+ − 0 −): distribution by dihedral angles (See Figure 5 for definitions).

for 180° and −60°, respectively. The conclusions of Fujiwara and co-workers were that all forms were equally populated at pH < 8.

As mentioned above, Fujiwara and co-workers found 40% population of the $C_\alpha C_\beta C_\gamma C = 180°$ rotamer of the glutamyl residue and assumed equal populations of the other two forms.

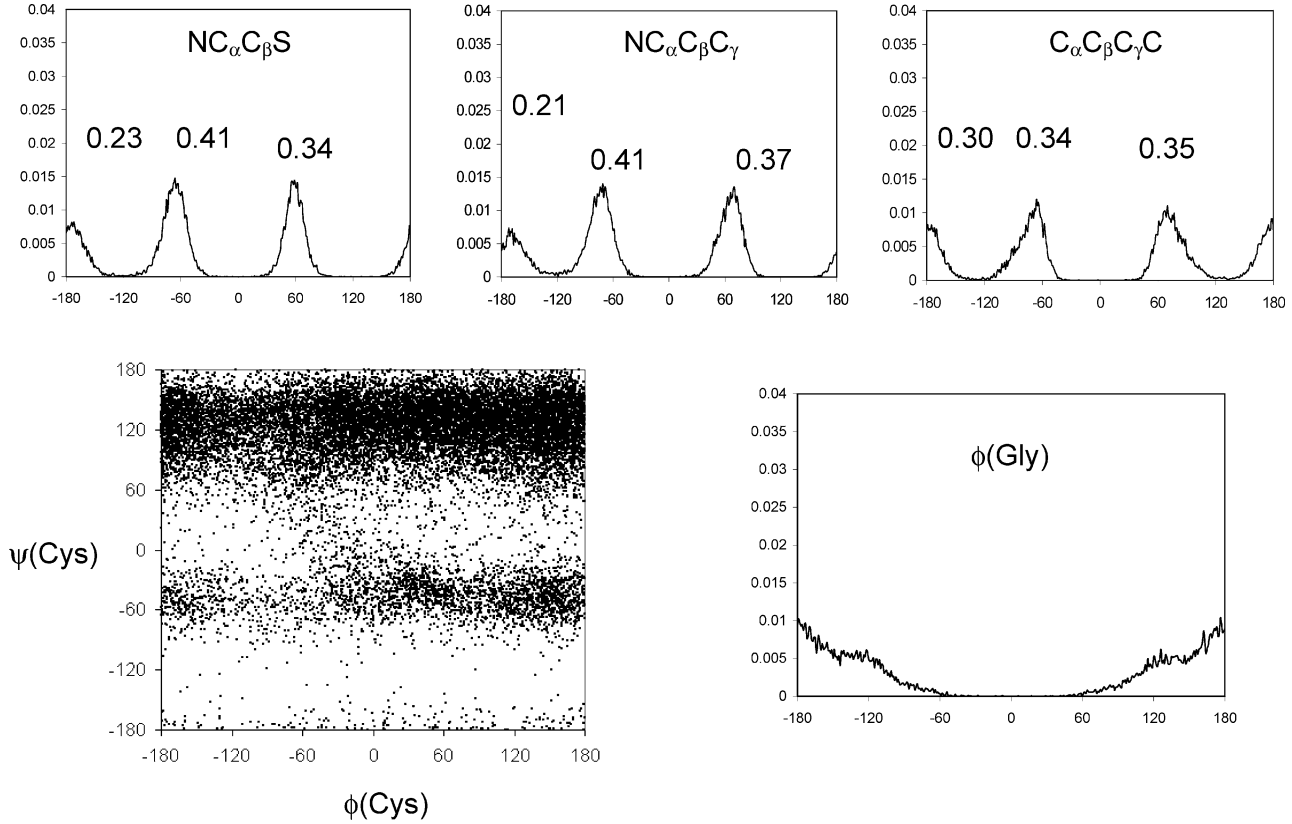

Figure 10. Structure **12**(0−0 −): distribution by dihedral angles (See Figure 5 for definitions).

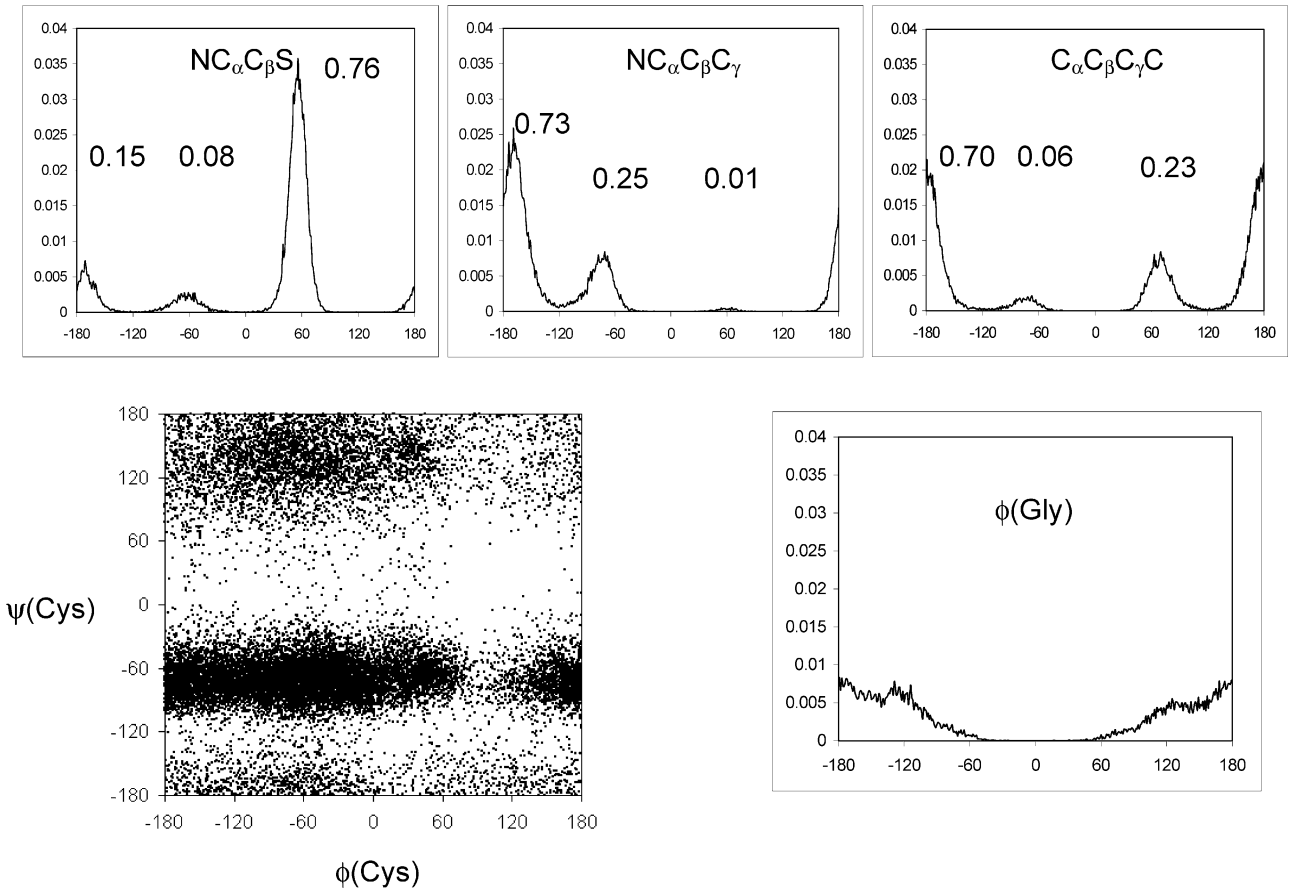

Figure 11. Structure **13**(+ − − −): distribution by dihedral angles (See Figure 5 for definitions).

The present analysis finds a greater population, 77%, of the 180° form, and approximately a 2:1 ratio of the +60° and −60° forms.

The two experimental studies and our simulations of GSH present three different pictures of the conformer distributions. Even given the fact that the results of the more recent study of

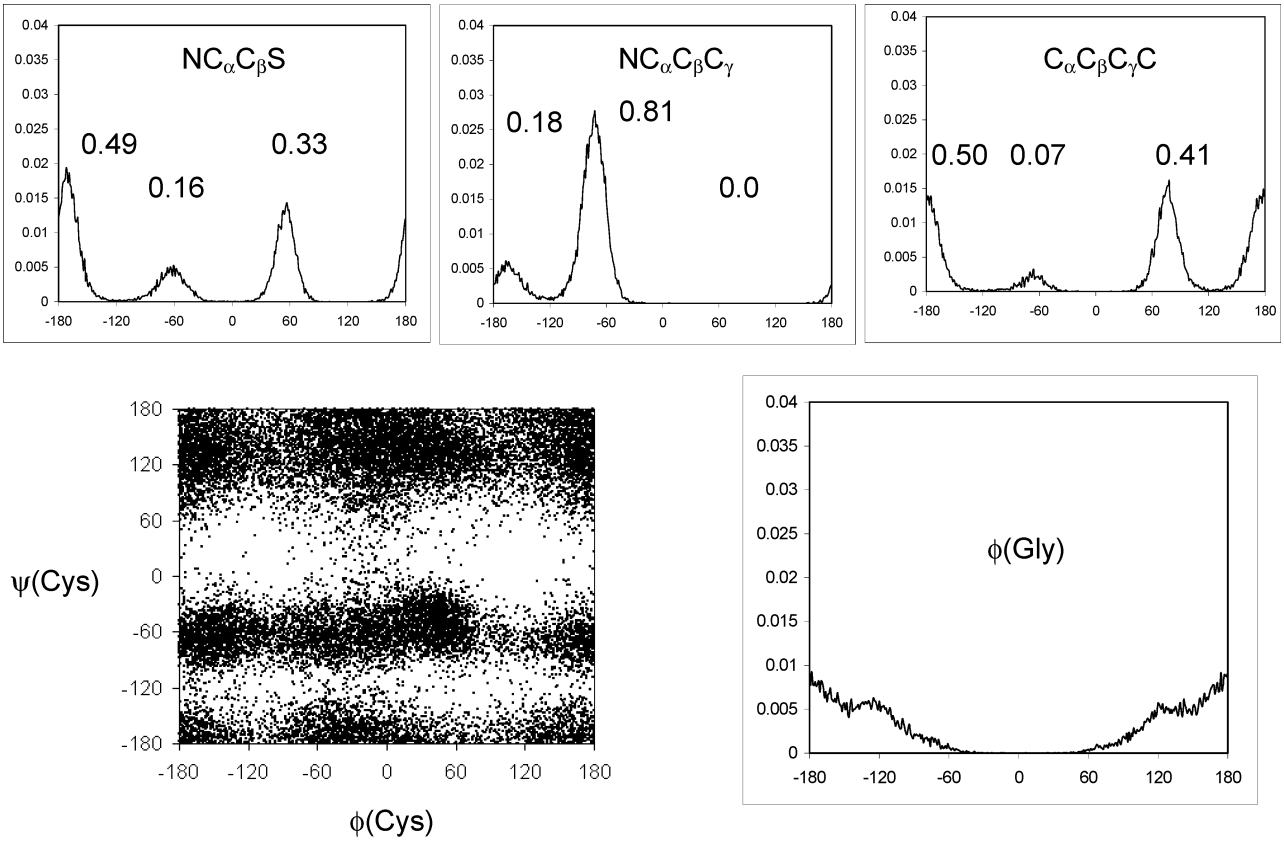

Figure 12. Structure **16**(0 − − −): distribution by dihedral angles (See Figure 5 for definitions).

York, et al.[14] will supersede the earlier work of Fujiwara[18] where the two overlap, the differences between the experimental conclusions and the present work are difficult to reconcile. From the simulation point of view, problems may arise if the trajectories are not adequately equilibrated, or if the force field is simply not up to the task. As mentioned above, we are confident that the individual species are well equilibrated over the 20 ns time span since repeated simulations from different starting structures of **1**(+ 0 0 0) and **6**(+ − 0 −) yield essentially the same populations of rotamers. As indicated in the Introduction, experience with Gromacs force fields suggests that the present Gromacs all-atom force field should perform acceptably. It is possible that the assumptions inherent in spin−spin coupling[18] or line-shape[14] analysis render the NMR technique to be less sensitive to torsional populations than was believed to be the case. Certainly the conclusions that all conformations about the butane-like $C_\alpha C_\beta C_\gamma C$ angle are equal, or that rotamer populations about the $NC_\alpha C_\beta S$ angle are independent of pH while the mix of species (including ionization of the thiol group) changes substantially over the range, are unexpected. Rather, the present simulation results are more reasonable in that anti rotamers tend to be favored over gauche rotamers, as expected, on the basis of qualitative steric arguments. The power of NMR as a structural tool has increased substantially in the 15 years since the last investigation. Perhaps the present work will spur a fresh examination of the solution structure of GSH.

Distribution of the Ramachandran Angles (Figures 5−12). No information is available from experimental sources pertaining to the distribution of the Ramachandran angles of GSH in aqueous solution. The three angles, ϕ(Cys), ψ(Cys), and ϕ(Gly), are defined in Figure 5, and the results of the simulations are displayed in Figures 6−12 for the seven species of primary interest (Figures 1 and 2). The present discussion will center primarily on the physiologically important form, **6**(+ − 0 −) (Figure 9).

The results for the cysteine residue are displayed as two-dimensional plots of each of the 20 000 points of each simulation. Point density is an excellent visual indicator of which regions of (ϕ,ψ) space are populated or avoided. In the case of **6**(+ − 0 −), and in most of the other species, the distribution clearly favors ψ(Cys) angles in the vicinity of +120° and −60°, with little dependence on ϕ(Cys). In **6**(+ − 0 −), as well as **1**(+ 0 0 0), **3**(+ 0 0 −), and **12**(0 − 0 −), there is a clear preference for the ψ(Cys) = 120° region. The data in Table 2 indicate that the most stable conformations of these species, shown in Figure 2, also adopt this orientation about ψ(Cys). The exceptions (Figures 7 and 11), in which the ψ(Cys) = −60° region is preferred, are of interest.

The distribution of ϕ(Gly) shown in Figures 6−12, for the most part, reflects the lack of chirality at the $^{\alpha}$C-center of Gly. Except in the case of species **3**(+ 0 0 −) and **6**(+ − 0 −), the distribution is almost symmetric about ϕ(Gly) = 0°. In the highly charged species, **12**(0 − 0 −), **13**(+ − − −), and **16**(0 − − −), the distribution is clustered in the vicinity of ϕ(Gly) = 180° (or −180°). The fully extended conformation probably arises due to mutual repulsion of the negatively charged groups in these molecules.

On the other hand, the distributions of ϕ(Gly) in **3**(+ 0 0 −) and in the physiologically relevant species, **6**(+ − 0 −) are highly unsymmetrical, being biased toward ϕ(Gly) = −60° and + 120°, respectively. The reason for this induced chirality in the case of **3**(+ 0 0 −) is due to the persistent intramolecular H-bonding discussed above, and as is evident from inspection of species **3a**(+ 0 0 −) in Figure 2. The reason for the asymmetric bias in **6**(+ − 0 −) is not as self-evident. This

orientation about ϕ(Gly) is also present in **6b**(+ − 0 −) (Figure 3 and Table 2) and may result from the steric requirements of the first solvation shell about the Gly carboxylate and the involvement of some of the tightly bound water molecules in secondary H-bonding to the N−H of the proximal amide group and/or to the C═O of the distal amide group.

Relationship to X-ray Structures of Free and Protein-bound GSH. The crystal structures of GSH[10] and its oxidized form, GSSG,[40] are given in Table 2 in terms of the major skeletal dihedral angles. Both structures are zwitterionic at the glutamyl end and neutral at the glycyl end, corresponding to structure **2**(+ − 0 0). Neither structure corresponds to any of the 160 solution conformations of **2**(+ − 0 0) identified by the cluster analysis. Relative to the solution structures, the crystal structure of GSH displays two anomalies. The $NC_\alpha C_\beta S$ angle of the Cys residue, 69.9°, falls into the most hindered, least populated (13%) orientation according to Figure 2. Second, the Ramachandran angle, ψ(Cys) = −3.0°, corresponds to a nearly eclipsed orientation that brings two N−H groups close together. This orientation is strongly avoided in solution according to Figure 2, but is brought about by strong intermolecular H-bonds in the crystal. The crystal structure of the oxidized form, GSSG, has a more favorable $NC_\alpha C_\beta S$ angle, but also has the nearly-eclipsed feature, with ψ(Cys) = 14.0°. Relaxing of the cluster analysis criterion to RMSD = 0.1 nm permits nearby conformations to be grouped into the same cluster, thereby reducing the apparent number of distinct "conformations". By the RMSD = 0.1 nm criterion, the number of clusters of **2**(+ − 0 0) is reduced to 47. While the crystal structure of GSH is still unassigned, that of GSSG is assigned to a cluster which by eq 1 is 6 kJ mol^{-1} higher than the most populated group. Alternatively, the RMSD = 0.075 nm criterion may be applied only to the backbone heavy atoms, thereby ignoring the orientation of the Cys side chain in the cluster analysis. By this criterion, the number of backbone-distinct conformations of **2**(+ − 0 0) is found to be 24, and both GSH and GSSG are assigned to clusters, 6.2 kJ mol^{-1} and 8.6 kJ mol^{-1}, respectively, higher than the most populated cluster. These values provide an indication of the minimum backbone strain energy that must be provided by crystal packing forces in order to bring these compounds out of aqueous solution.

The structures of a number of enzyme-bound glutathione species are listed in Table 2. All of the structures are partially exposed to the aqueous environment and the conformations are determined by competitive interactions with the solvent and the protein matrix to which they are bound. All are zwitterionic at the glutamyl end and deprotonated at the glycyl end, and correspond to the most populated charged state, **6**(+ − 0 −), at physiological pH. Excluding GSH conjugates, 22 entries, including two determined by NMR analysis, are found in the Brookhaven National Laboratory Protein Data Bank (PDB).[41] A variety of these are listed in Table 2, identified by their PDB ID codes. The GSH substrates are complexed to the enzyme noncovalently by H-bonding and electrostatic interactions (1gsy, 1ljr, 6gss, 7gss, 19gs, 1fhe, 6gsy, 1hnl, 1jzr, 1k0n, 1gsa, and 1pd2), or are also covalently bound through a disulfide linkage (1f2e, 1pmt, 2pmt, 1flj, 1b4q, and 3grx).

Of the ten glutathione S-transferase complexes, the structures of GSH in eight are either equivalent to low-energy solution conformations of **6**(+ − 0 −) (1f2e, 1ljr, 1pmt, and 2pmt, designated by the = sign in Table 2), or differ only in the Cys side chain orientation from low-energy conformations (1 g2y, 6gss, 7gss, and 19gs, designated by the ≈ sign in Table 2). Two of the complexes with glutathione S-transferase, 1fhe and 6gsy, do not correspond to any of the solution-simulation structures. Both have the Ramachandran angles of the Cys moiety (Table 2) in regions which are not populated in solution (Figure 9). As in the case of the crystal structures of GSH and GSSG, structure 6gsy has a nearly eclipsed orientation of ψ-(Cys). One of the two GSH−URE2 protein complexes (involved in gene regulation), 1jzr, corresponds closely to **6h**(+ − 0 −), which is 3.5 kJ mol^{-1} higher than the most stable conformation. The backbone of the other, 1k0n, corresponds to **6c**(+ − 0 −), but the orientation of the Cys side chain places the SH group in the most hindered orientation relative to the backbone ($NC_\alpha C_\beta S \approx 60°$, see Figure 9). The conformation of GSH in the complex with glutaredoxin III (involved in electron transport), 3grx, corresponds closely to the solution conformation, **6e**(+ − 0 −), despite being covalently linked through the Cys side chain. On the other hand, the covalently linked GSH in the complex with human thiol transferase (an oxidoreductase), 1b4q, has the Cys moiety in a conformation that is not populated in aqueous solution (compare the $NC_\alpha C_\beta S$, ϕ(Cys), and ψ(Cys) values from Table 2 with the plots in Figure 9). In the case of both the lysozyme-bound complex, 1hnl, in which the GSH is noncovalently bound, and the carbonic anhydrase III-complex (a lyase), 1flj, in which the GSH is covalently linked, the orientation of the glutamyl side chain is in a highly hindered orientation ($NC_\alpha C_\beta C_\gamma \approx 60°$) which is totally unpopulated in solution. The two ligase-bound complexes, 1pd2 (hematopoietic prostaglandin D synthase) and 1gsa (glutathione synthase), in both of which the GSH is noncovalently bound, have the backbone of GSH in a low energy conformation.

In summary, the conformations of GSH in many of the enzyme-bound complexes correspond to the more stable conformations of **6**(+ − 0 −), indicating that there is almost no free energy hurdle to be overcome in order to form the enzyme-bound complex. However, in some, the local bonding environment, whether covalent or not, forces the GSH moiety into a conformation not populated in aqueous solution.

Proximity of the Thiol SH and $^\alpha$C−H of the Glutamyl Residue. We return to the original question of whether the thiol S and $^\alpha$C−H(Glu) groups can approach each other sufficiently closely so that H-atom transfer may take place between the two centers in the event that a radical is generated at one site or the other. Such an H-atom transfer has been observed[5,6] in experiments carried out at pH = 10, and the energetic feasibility of the process was demonstrated by ab initio calculations.[8] In the present case, it must be assumed that the conformational behavior of a thiyl radical in solution would be adequately represented by that of a thiol or thiolate group in the simulations. In Figure 13 is shown the distribution of the S to H (of $^\alpha$C−H(Glu) distances of the species that would be populated at pH = 10, namely **12**(0 − 0 −), **13**(+ − − −), and **16**(0 − − −). The populations of these species are approximately 10%, 15%, and 75%, respectively. Figure 13 also shows the distribution for the physiologically important species, **6**(+ − 0 −). Bins in the histogram that correspond to a distance of less than 4 Å (bins 1−4) represent conformations in which the two groups are virtually in contact. Species **13**(+ − − −) is unique among the species described in Figure 13 in that it spends considerably more time, 13%, with the sulfur and the H of the glutamyl $^\alpha$C-site within 4 Å of each other. It is the only species with both the sulfur and the glutamyl $^\alpha$C-amino group ionized. The close proximity of the S to the H is a side effect of the attraction between the two ionic groups. Such an attraction was observed in the earlier discussion of the case of **3**(+ 0 0 −) (Figure 4 and text above).

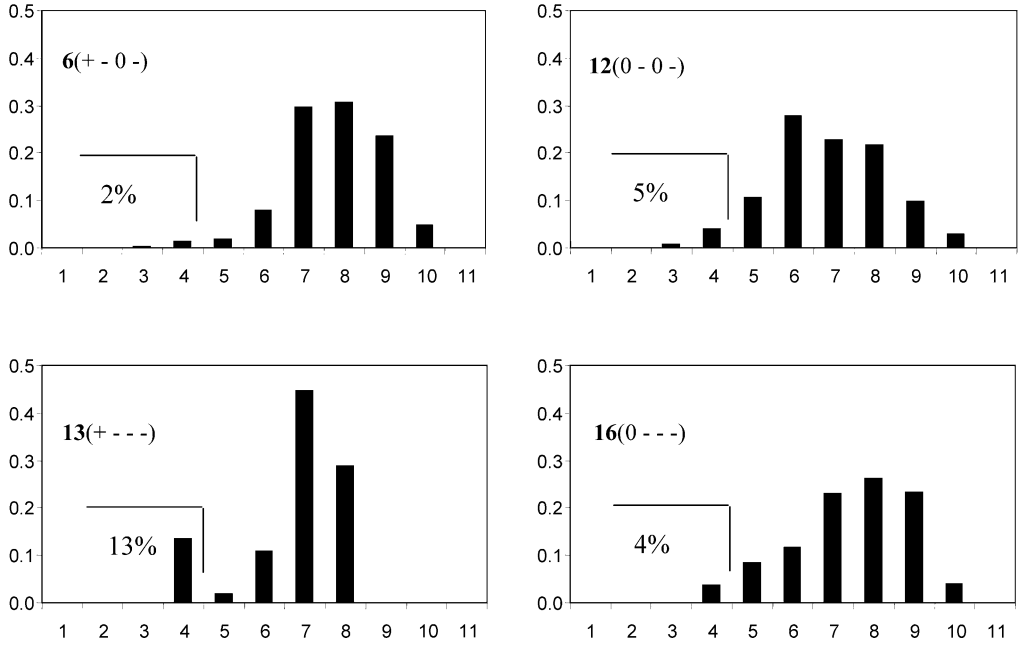

Figure 13. Histograms of S to H (of $^{\alpha}$C−H(Glu) distances for **6**(+ − 0 −), **12**(0 − 0 −), **13**(+ − − −), and **16**(0 − − −). Numbers in % indicate percent of the total simulation time spent at distances less than 4 Å.

Conclusions

Sixteen charge states, each with potentially hundreds of conformations, are available to the physiologically ubiquitous antioxidant, glutathione (GSH), in aqueous solution. Molecular dynamics simulations over 20 ns with the Gromacs force field, coupled with cluster analyses of the trajectories, have generated the populations and relative free energies of the lowest energy conformations of each charged state. The simulations show that GSH is very flexible and does not adopt a strongly preferred conformation at any pH. The distribution about the principal torsion angle derived from the simulations agrees only marginally with that deduced from NMR spectroscopic studies at different values of pH. The NMR results have been interpreted as evidence of similar populations of the three staggered rotameric forms of the Cys and Glu side chains, while the simulations reveal lower populations for gauche forms. In most species, the lowest populations were found for the sterically hindered gauche−gauche orientation about the $C_{\alpha}-C_{\beta}$ bond in both residues.

Comparison of the solution conformations with the solid-state crystallographic structures of GSH and the oxidized form, GSSG, shows that crystal packing and intermolecular H-bonding interactions force the GSH skeleton into a conformation that is not seen in solution. The same is true for some of the enzyme-bound GSH structures, although in the majority of the examples in the Brookhaven Protein Data Bank, the bound GSH has a conformation that is either the same or similar to that free in solution.

The distribution of the separation of the Cys S atom from the Glu $^{\alpha}$C−H bond was monitored over the course of the 20 ns simulations of **12**(0 − 0 −), **13**(+ − − −), and **16**(0 − − −), the three most abundant species at pH = 10. These are the conditions under which H atom transfer was observed to occur from the Glu $^{\alpha}$C−H bond to a thiyl radical of the Cys moiety of GSH. Species **13**(+ − − −), which is in 15% abundance, is unique among the species in that it spends 13% of the time with the sulfur and the H in close contact, i.e., within 4 Å of each other. By contrast, neither **12**(0 − 0 −) nor **16**(0 − − −) spends more than 5% of the simulation time with the S and H in close proximity. At physiological pH, the dominant species is **6**(+ − 0 −), in which the S and H are in contact only 2% of the time. The results suggest that the radical reaction is more efficient at alkaline pH, and probably occurs via **13**(+ − − −).

Acknowledgment. The financial support of the Natural Sciences and Engineering Council of Canada (NSERC) is gratefully acknowledged. We are also grateful to the Center of Scientific Computing in Espoo, Finland, for providing computing power. We thank Dr. Craig Shepherd and Dr. Jacqueline Berges for valuable discussions in the early stages of this work.

References and Notes

(1) Moran, L. A.; Scrimgeour, K. G.; Horton, H. R.; Ochs, R. S.; Rawn, J. D. *Biochemistry*, 2nd ed.; Prentice Hall: Englewood Cliffs, NJ, 1994.
(2) Bains, J. S.; Shaw, C. A. *Brain Res. Brain Res. Rev.* **1997**, *25*, 335−358.
(3) Rauk, A.; Yu, D.; Taylor, J.; Shustov, G. V.; Block, D. A.; Armstrong, D. A. *Biochemistry* **1999**, *38*, 9089−9096.
(4) Rauk, A.; Yu, D.; Armstrong, D. A. *J. Am. Chem. Soc.* **1998**, *120*, 8848−8855.
(5) Zhao, R.; Lind, J.; Merényi, G.; Eriksen, T. E. *J. Am. Chem. Soc.* **1994**, *116*, 12010−12015.
(6) Zhao, R.; Lind, J.; Merényi, G.; Eriksen, T. E.. *J. Chem. Soc., Perkin Trans. 2* **1997**, 569−574.
(7) Grierson, L.; Hildebrand, K.; Bothe, E. *Int. J. Radiat. Biol.* **1992**, *62*, 265−277.
(8) Rauk, A.; Armstrong, D. A.; Berges, J. *Can. J. Chem.* **2001**, *79*, 405−417.
(9) Wright, W. B. *Acta Crystallogr.* **1958**, *11*, 632−642.
(10) Gorbitz, C. H. *Acta Crystallogr.* **1987**, *41*, 362.
(11) Oakley, A. J.; Lo Bello, M.; Battistoni, A.; Ricci, G.; Rossjohn, J.; Villar, H. O.; Parker, M. W. *J. Mol. Biol.* **1997**, *274*, 84−100.
(12) Raghunathan, S.; Chandross, J.; Kretsinger, R. H.; Alliston, T. J.; Penington, C. J.; Rule, G. S. *J. Mol. Biol.* **1994**, *238*, 815−832.
(13) Rabenstein, D. L. *J. Am. Chem. Soc.* **1973**, *95*, 2797−2803.
(14) York, M. J.; Beilharz, G. R.; Kuchel, P. W. *Int. J. Peptide Protein Res.* **1987**, *29*, 638−646, and references therein.
(15) Nicotra, M.; Paci, M.; Sette, M.; Oakley, A. J.; Parker, M. W.; Lo Bello, M.; Caccuri, A. M.; Federici, G.; Ricci, G. *Biochemistry* **1998**, *37*, 3020−3027, and references therein.
(16) McCallum, S. A.; Hitchens, T. K.; Torborg, C.; Rule, G. S. *Biochemistry* **2000**, *39*, 7343−7356, and references therein.
(17) Laurence, P. R.; Thomson, C. *Theor. Chim. Acta* **1980**, *57*, 25−41.

(18) Fujiwara, S.; Formicka-Kozlowska, G.; Kozlowski, H. *Bull. Chem. Soc. Jpn.* **1977**, *50*, 3131−3135.
(19) Smith, L. J.; Mark, A. E.; Dobson, C. M.; van Gunsteren, W. F. *Biochemistry* **1995**, *34*, 10918−10931.
(20) Polverini, E.; Casadio, R.; Neyroz, P.; Masotti, L. *Arch. Biochem. Biophys.* **1998**, *349*, 225−235.
(21) Shepherd, C. M.; Schaus, K. A.; Vogel, H. J.; Juffer A. H. *Biophys. J.* **2001**, *80*, 579−596.
(22) Daura, X.; Juan, B.; Seebach, D.; van Gunsteren, W. F.; Mark, A. E. *J. Mol. Biol.* **1998**, *280*, 925−932.
(23) Bonvin, A. M. J. J.; van Gunsteren, W. F., *J. Mol. Biol.* **2000**, *296*, 255−268.
(24) Mogilner, I. G.; Ruderman, G.; Grigera, J. R. *J. Mol. Graph. Model.* **2002**, *21*, 209−213.
(25) van der Spoel, D., *Biochem. Cell Biol.* **1998**, *76*, 164−170.
(26) Duneau, J. P.; Garnier, N.; Cremel, G.; Nullans, G.; Hubert, P.; Genest, D.; Vincent, M.; Gallay, J.; Genest, M. *Biophys. Chem.* **1998**, *73*, 109−119.
(27) Körtvélyesi, T.; Kiss, G.; Murphy, R. F.; Penke, B.; Lovas, S. *J. Mol. Struct. (THEOCHEM)* **2001**, *545*, 215−223.
(28) Zhang, Z.; Zhul, Y.; Shi, Y. *Biophys. Chem.* **2001**, *89*, 145−162.
(29) Möhle, K.; Hofman, H.-J. *J. Mol. Struct. (THEOCHEM)* **1995**, *339*, 57−65.
(30) Labrou, N. E.; Mello, L. V.; Ridgen, D. J.; Keen, J. N.; Findlay, J. B. C. *Peptides* **1999**, *20*, 795−801.
(31) Kolmodin, K.; Åqvist, J. *FEBS Lett.* **2000**, *465*, 8−11.
(32) Berendsen, H. J. C., van der Spoel, D. and van Drunen, R. 1995. GROMACS: a Message − passing Parallel Molecular Dynamics Implementation. *Comp. Phys. Commun. 91*, 43−56.
(33) We thank Dr. Craig Shepherd for carrying out this simulation.
(34) Berendsen, H. J. C., Postma, J. P. M., van Gunsteren, W. F. and Hermans, J. in: *Intermolecular Forces* (Pullman, B., Ed.), Reidel: Dordrecht; pp 331−342 1981.
(35) Berendsen, H. J. C.; Postma, J. P. M.; DiNola, A.; Haak, J. R. *J. Chem. Phys.* **1984**, *81*, 3684−3690.
(36) (a) Darden, T. A.; York, D. M.; Pedersen, L. G. *J. Chem. Phys.* **1995**, *103*, 8577−8593. (b) Essmann, U.; Perera, L.; Berkowitz, M. L.; Darden, T. A.; Lee, H.; Pedersen, L. G. *J. Chem. Phys.* **1993**, *98*, 10089−10092.
(37) Hess, B.; Bekker, H.; Berendsen, H. J. C.; Fraaije, J. G. E. M. 1997. LINCS: a Linear Constraint Solver for Molecular Simulations. *J. Comput.Chem. 18*, 1463−1472.
(38) Miyamoto, S.; Kollman, P. A. 1992. SETTLE: an Analytical Version of the SHAKE and RATTLE Algorithms for Rigid Water Models. *J. Comput. Chem. 13*, 952−962.
(39) (a) Daura X.; van Gunsteren W. F.; Mark, A. E. *Proteins: Structure, Function, and Genetics* **1999**, *34*, 269−280. (b) Daura X.; Gademann, K.; Jaun, B.; Seebach D.; van Gunsteren W. F.; Mark, A. E. *Angew. Chem., Int. Ed.* **1999**, *38*, 236−240.
(40) Jelsch, C.; Didierjean, C. *Acta Crystallogr.* **1999**, *C55*, 1538−1540.
(41) The PDB website is http://www.rcsb.org/pdb/